(Received 6 June 2024, Accepted 31 July 2024, Scheduled 14 August 2024)

Designing Magnetic Coupler of Static Wireless Power Transfer System for Thermal Reduction by Using Silicon-Cobalt Wafer

Umar Farooq[1,*], Jiropast Suakaew[2], Poramed Wongjom[3], Latif Jan[4], Maryam[3], and Wanchai Pijitrojana[1,*]

[1]*Electrical and Computer Engineering Department, Thammasat School of Engineering, Thammasat University Rangsit Campus Klongluang, Pathum Thani 12120, Thailand*
[2]*Department of Integrated Engineering, Faculty of Engineering, Pathumwan Institute of Technology 833 Rama Road, Pathumwan, Bangkok 10330, Thailand*
[3]*Division of Physics, Faculty of Science and Technology Thammasat University Rangsit Campus Klongluang, Pathum Thani 12120, Thailand*
[4]*Department of Computer Science, Iqra National University Peshawar, Pakistan*

ABSTRACT: Wireless power transfer (WPT) for electric vehicles (EV) is a promising technology that can help with e-mobility because of its convenience and ability to reduce range anxiety issues. The safety concerns of such systems have received a lot of attention recently. Magnetic coupler is the most important component of WPT systems in terms of thermal safety as its temperature rises because of power outages during the charging process, which could cause damage to the surroundings and other components associated with the system. This article proposes a new thermal and magnetic coupler design by utilizing a Silicon-Cobalt wafer using the Spin Seebeck effect (SSE) phenomenon fabricated through the sputtering technique which can enhance the efficiency of the transmission coil as well as act as a heat exchanger to remove the heat from the coil as well as reduce temperature with the design model.

1. INTRODUCTION

Electric vehicles (EVs) have gained much popularity throughout the modern world due to their increased energy efficiency and ability to lower pollution and carbon dioxide emissions [1, 2]. Compared to plug-in electric vehicles, wireless electric vehicles are one of the most promising technologies in recent times having the potential to resolve the problems and challenges that occur in conductive charging including range anxiety, battery capacity cost, and size of the cables utilized during charging and operating of the vehicle [3–6]. Ref. [7] has addressed the study of EV technology and the advances that have been made in substantial fields like batteries, charging, electric motors, and charging infrastructure. Static wireless charging and dynamic wireless charging are the two basic categories into which WPT systems can be divided [8, 9]. When using the static wireless charging technique, a vehicle is parked over a charging mechanism that is embedded or mounted alongside a platform known as the transmitter (Tx) [10]. A matching charging pad that is mounted on the vehicle's underside, known as the receiver (Rx), detects the transmission signal and charges the car as illustrated in Fig. 1.

There are several locations for the transmitter and receiver that are suitable for wireless EV charging: One method is to bury the transmitter coils underground and place the receiver coils beneath the EV's chassis. The EV can then be charged by driving the vehicle over the below-ground transmitter coils. Another option is to install the transmitter coils in the walls of the garage or charger infrastructure and the receiver coils vertically just behind the front bumper or grilles (for example, replacing the radiators in ICE vehicles) [10]. The car charges when it is parked facing these embedded transmitter coils. Compared to conductive charging systems, WPT technique's main limitation is its lower power transfer efficiency over longer distances. Coupling coefficient (CC) has been highlighted in the literature as a crucial area of study for WPT systems since it offers the maximum output power and drastically impacts the system's overall efficiency [11].

The loosely coupled (LC) transformer's size at a specific air gap establishes the CC, hence the coil's geometry, shape, number of turns, width, and distance between turns contribute to the WPT system's overall efficiency. Many resonant circuit compensation topologies and control approaches for the inverters and converters on either end of the charger have been examined in a wide range of literature that can assist with the development of WPT systems. For the transmitter and receiver side resonant circuits, there are two common topologies: parallel and series connected circuits and series circuits [12, 13]. Each compensation topology has pros and cons of its own. The selection must be made in compliance with the application's specifications [14–16]. For the widely used resonant topologies, the authors [17, 18] have addressed the magnetic coupling effect as a general design technique.

* Corresponding authors: Umar Farooq (Umar.far@dome.tu.ac.th); Wanchai Pijitrojana (pwanchai@engr.tu.ac.th).

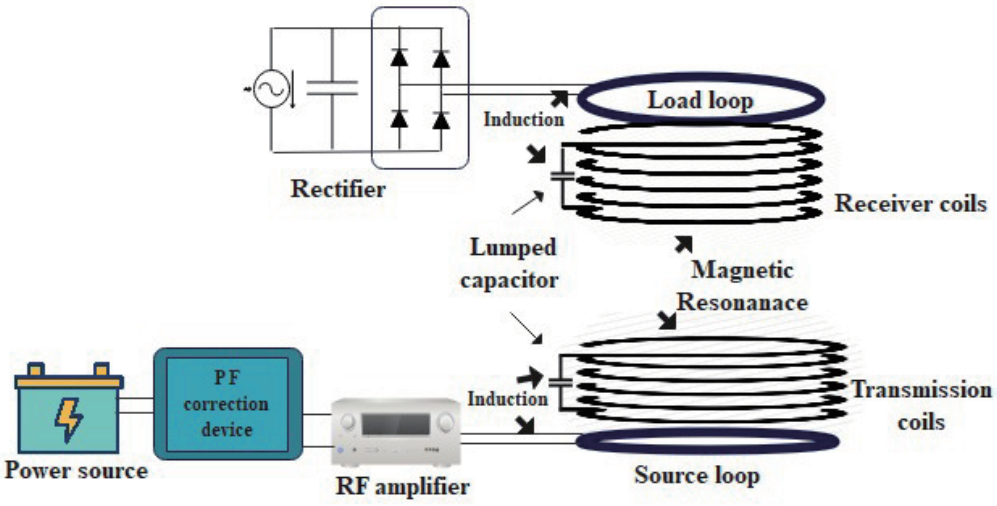

FIGURE 1. Transmitting and receiver coil magnetic coupling (MC).

Nevertheless, losses in wireless charging system (WCS) contribute to the emission of heat, which increases the temperature and contributes to likely risk concerns [19]. The magnetic coupler's effectiveness could be adversely affected by an increase in temperature. Thus, to avoid more than the thermal limits, the system's steady-state temperature must be established during the WCS design process [20]. On the contrary, the WCS vehicle assembly (VA) and ground assembly (GA) are normally housed in boxes. The volume of the WPT system is increased by cooling mechanisms like liquid cooling, air cooling, or composite phase-change materials, which makes it unable to meet the high compactness requirement [21–24]. In real-world applications, it is preferable to maximize the magnetic coupling coefficient and transmission efficiency while minimizing the volume and weight of the magnetic coupler. For this reason, it is essential to concentrate on thermal design and WCS optimization.

The component losses have been the source of the thermal energy in the WPT EV magnetic coupler. For this reason, developing a precise loss computation model is necessary for thermal analysis. Establishing the loss model requires calculating the losses in the litz coil. Litz wire, which is made up of several twisted, insulated strands of fine copper wire, lowers the coil's skin effect losses in high-frequency magnetic fields [25]. When it performs at lower frequencies, the proximity effect's influence is often ignored [26], with only the existence of conduction resistance taken into account. However, in high-frequency systems, this method may result in important errors.

In [27], the average magnetic field strength of each turn's cross-section in the litz coil is determined via the finite element approach (FEM) software. Following this, using theoretical formulas, the coil's proximity effect resistance is calculated. A more accurate measurement of the internal resistance of the litz coil can be achieved through modelling the litz wire and obtaining formulas for its ac resistance using analytical calculation techniques like the Biot-Savart law and Maxwell's equations [28, 29]. An improved approach for calculating ac resistance is utilized in [30], which retains good accuracy even in situations where the litz coil has sparse winding. The optimized method is performed automatically by the particle swarm optimization algorithm. The thermal network method (TNM), a thermal-electric analog analysis technique, offers quick and effectively manageable calculations for the thermal analysis of WCS. Its ability to entirely understand temperature distribution and hot spot locations is limited, though. As such, it might not be appropriate for applications requiring real-time temperature monitoring. Electric motor and transformer thermal analyses frequently employ TNM [31, 32]. To analyze temperature characteristics qualitatively, an improved thermal resistance system for the magnetic coupler was established, and the experimental results showed that the thermal simulation was reliable [33].

The thermal hazards associated with angular and horizontal displacements were analysed in [34] which determine the risk levels, and four evaluation criteria were put forth. In high-power systems, consideration needs to be made for the heating generated by eddy current losses in metal objects with an air gap. These things frequently have temperatures higher than those of magnetic couplers resulting in higher hazards. In [35], force-air cooling can be used to strengthen WCS's thermal reliability. This can be seen from Moghaddami and Sarwat [36] via a time-varying model of CFD simulations using multiple physical fields. In addition, cardiac pacemaker prototype selection and safety assessment utilize thermal analysis [37, 38]. To enhance the WCS's performance, the magnetic coupler needs to be maximized after the thermal and loss analysis models have been established. With the optimization objective of kQ, the inner and outer diameters of the coil, its mutual inductance, and its number of turns are determined as optimization parameters in [39]. New design criteria have been identified as optimization aims in [26] and [40] complying with an analysis of the relation between coil parameters and efficiency. The temperature of the magnetic coupler is rarely included in the optimization objectives in literature, mainly focusing on electromagnetic field aspects. The surface power loss density has

been used in [41] and [42] as a constraint to filter towards some feasible options, but the temperature is not considered as an optimization goal.

Combining the energy conservation rule with an analysis of the heat transfer generated during operation, which is grounded in basic heat transfer theories and fluid mechanics, allows for the calculation of the temperature increase surrounding the coil. There are three methods for transferring heat: conduction, convection, and radiation. The fundamental law of heat conduction originates from Fourier's law, which quantifies the amount of heat that travels over a given area for a given length. The conduction heat flow rate is determined by the temperature gradient and the cross-sectional area perpendicular to the direction of heat conduction. Alternatively, the expression can be stated as follows:

$$Q_1 = -\lambda A_1 \frac{dt}{dx} \tag{1}$$

in which A_1 is the cross-sectional area in the vertical thermal conductivity direction (m^2), λ the material's thermal conductivity (W/(m·°C)),Q_1 the heat transfer heat flow (W), and the temperature gradient along the isothermal surface average to the direction (°C/m). A negative sign indicates that the direction of heat transmission is the opposite of the temperature gradient. The amount of heat dissipation via heat transfer can be increased by using a material with a high thermal conductivity and increasing it. Eq. (2), given below, compares convection heat transfer. Q_2 is the convective heat exchange quantity (W), and hc is the convective heat exchange coefficient (W/(m·°C). The effective convective heat exchange area of the contact surface, or A_2, is measured in units of (m^2). The cooling fluid temperature, or t_f, is measured in units of (°C); the solid surface temperature, or t_w, is measured in units of (°C). It makes it clear that increasing the convective heat transfer area and coefficient are two ways to improve convective heat transfer

$$Q_2 = h_c A_2 \left(t_w - t_f\right) \tag{2}$$

The means of releasing energy from an object to its surroundings by electromagnetic waves is known as radiant heat transfer. Anything that is warmer than absolute zero both absorbs and releases energy from the surrounding environment at a particular wavelength into space. When there is a temperature difference between the objects, mutual thermal radiation happens; otherwise, no thermal radiation will occur. Eq. (3) can be used to determine the radiation heat exchange between the surfaces of two objects.

$$Q_3 = \delta_\circ A_3 \epsilon_{xt} F_{12} \left(T_1^4 - T_2^4\right) \tag{3}$$

Equation (3) uses Q_3 to represent the convective heat exchange rate. The Stephan-Boltzmann constant ($\delta\_^\circ$) is 5.67×10^{-8} W/(m^2·K^4). The system emissivity is denoted by ϵ_{xt}. The surfaces of the high- and low-temperature objects are represented by ε_1 and ε_2. F_{12} is the angular coefficient connecting surface 1 and surface 2, and their absolute temperatures (K) are T_1^4 and T_2^4. The object's surface area used for radiative heat exchange is denoted by A_3. The equation demonstrates that in order to enhance the radiation heat exchange between the object surfaces, one can increase the emissivity of the heat source surface, the angle coefficient from the hot surface to the cooling surface, and the surface area of the increased radiation heat exchange.

1.1. Main Works and Contributions

This article shows a thermal reduction for the magnetic coupler in WCSs after evaluating the previously mentioned information. The method develops a heat dissipation model to design a high-performance wireless charging system. Also, the work in this article can contribute to the expansion of the WCS's present research. The following are the principal and basic contributions.

1. Considering the Spin Seebeck Effect (SSE) phenomenon a Silicon-Cobalt wafer connected with the Copper wiring is designed and fabricated through laser cutting and sputtering technique, and SSE of the designed wafer is measured through the low-cost SSE measuring instrument.

2. Set up a WPT system for analysing the temperature of the magnetic coupler with and without the designed wafer.

3. Utilize the fabricated design wafer with a static wireless power transfer system, and analyze temperature with the system to limit the amount of heat from the magnetic coupler.

The rest of the article is organized as follows. Section 2 explains the principal Spin Seebeck effect (SSE). Section 3 provides detailed information about the design and wafer fabrication through the sputtering technique and its SSE analysis and results. Section 4 contains a detailed static WPT experiment setup with the utilization of the designed fabricated wafer with the system. Section 5 shows the model experiments and their results with and without the utilization of the design wafer and heat sink as well as the simulation analysis with and without placing samples utilizing the SSE phenomenon. In the end, Section 6 concludes the article.

2. COBALT AND SPIN SEEBECK EFFECT

Due to the common and abundant availability of heat, it is necessary to utilize thermal energy sources like waste heat recovery and solar heat power generation efficiently to realize a sustainable society in the future. One of the more promising methods for efficiently utilizing heat is thermoelectric generation, which allows for the direct conversion of thermal energy into electrical power [43–45]. The Seebeck effect, identified by T. J. Seebeck in 1821, is the fundamental basis for a majority of commonly utilized thermoelectric-generating technologies [46, 47]. The term "Seebeck effect" describes the creation of an electric field (E_{SE}) in a conductor due to a temperature gradient ∇T with the direction of E_{SE} parallel to the temperature change. Spin voltage is also defined as the spin current potential, denoted by μ''_1 μ_2 where μ_1 and μ_2 stand for the electrochemical potentials for spin-up and spin-down electrons, respectively. As two conductors with different S values were naturally present in one magnet, spin-up and spin-down conduction electrons in a metallic magnet have significantly vary-

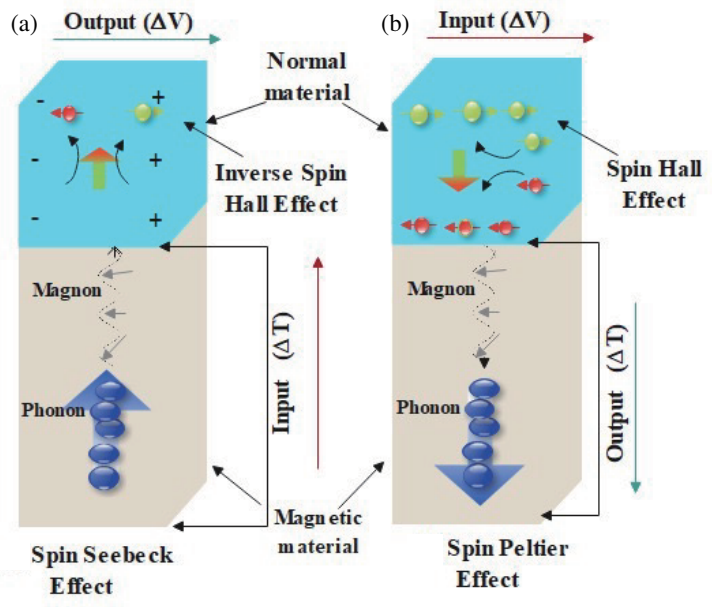

FIGURE 2. (a) Spin Seebeck Configuration and (b) Spin Peltier effect because they are both reciprocal to each other because spin pumping is the reciprocal of spin accumulation and ISHE is the reciprocal of SHE.

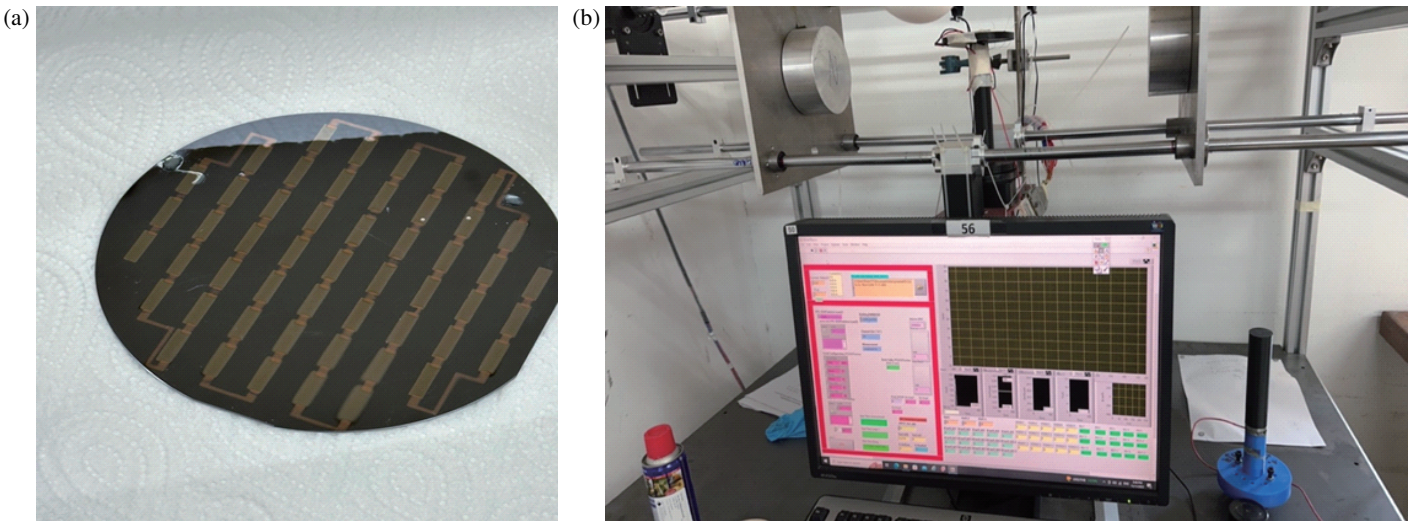

FIGURE 3. (a) Silicon cobalt wafer connected via copper winding through sputtering technique. (b) SSE measurement instrument for Si-cobalt wafer.

ing scattering rates and densities which leads to different Seebeck coefficients. Therefore, when a metallic magnet comes into contact with a temperature gradient, it must generate different electron-driving powers across different spin channels along the gradient [48–51]. Typically, SSE is measured in a junction made up of paramagnetic (NM) and ferromagnetic materials (FM). The spin-orbit interaction in the NM layer generates the inverse spin Hall effect (ISHE) to electrically detect the spin current inserted in the NM layer (SSE voltage) [52–56]. The NM usually comprises a heavy metal, mainly Pt, to enhance detection efficiency [57, 58]. The following equation provides the ISHE-driven electric field (E_{ISHE}).

$$E_{ISHE} = \theta_{SH}\rho\left(J_S \times \sigma\right), \tag{4}$$

where θ_{SH} and ρ stand for the NM layer's electric resistivity and spin Hall angle. The spin polarisation (parallel to the FM magnetization) and the spin current injected into NM across the FM/NM interface (parallel to ∇T) are denoted by spatial directions J_S and σ, respectively. The reciprocal of the SSE, the spin Peltier effect (SPE), describes the generation of heat current in a linear response to spin current injection. Seebeck and Peltier spin configurations are shown in Figs. 2(a) and (b). As SHE is the Onsager reciprocal of the ISHE and spin pumping is the Onsager reciprocal of spin accumulation, they are reciprocals of one another.

In fields where high-temperature capabilities, energy storage, process efficiency, and environmental advantages are crit-

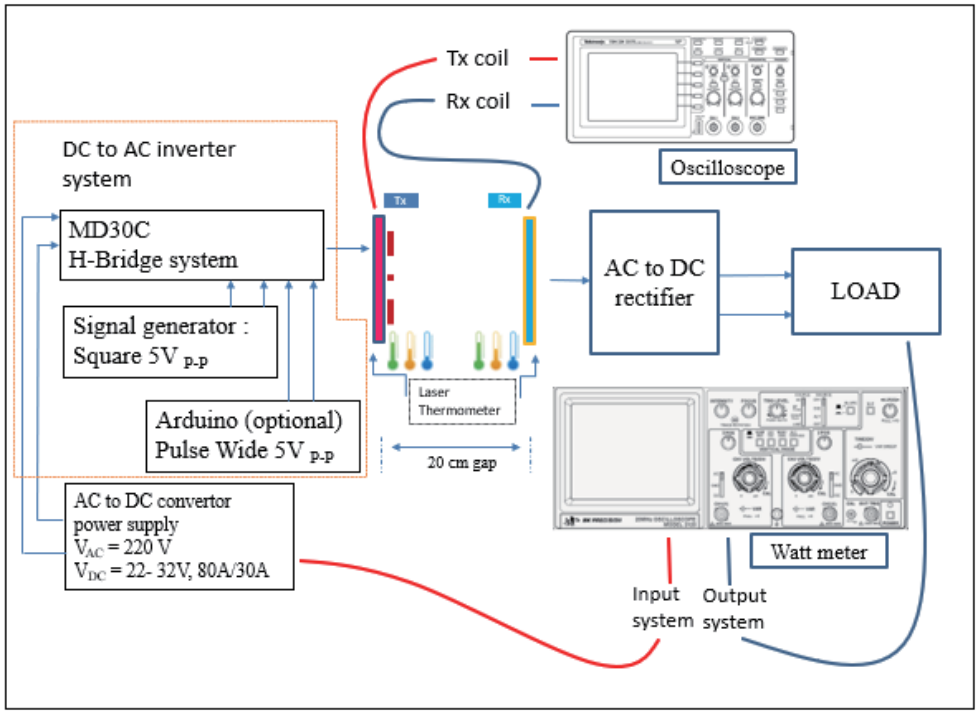

FIGURE 4. Layout diagram of WPT system.

(a)

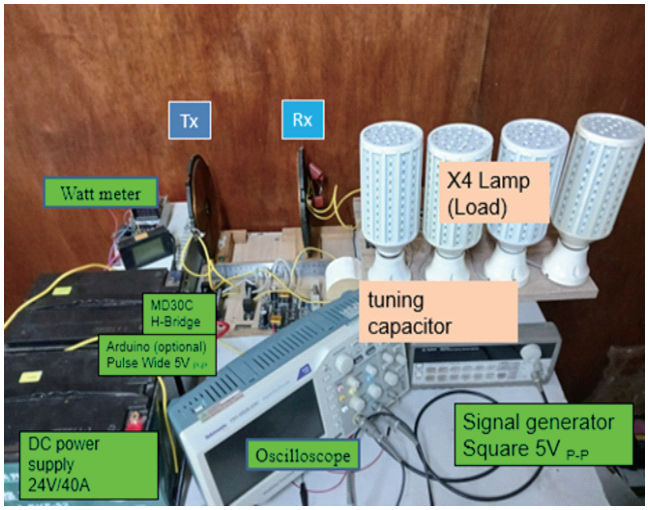

(b)

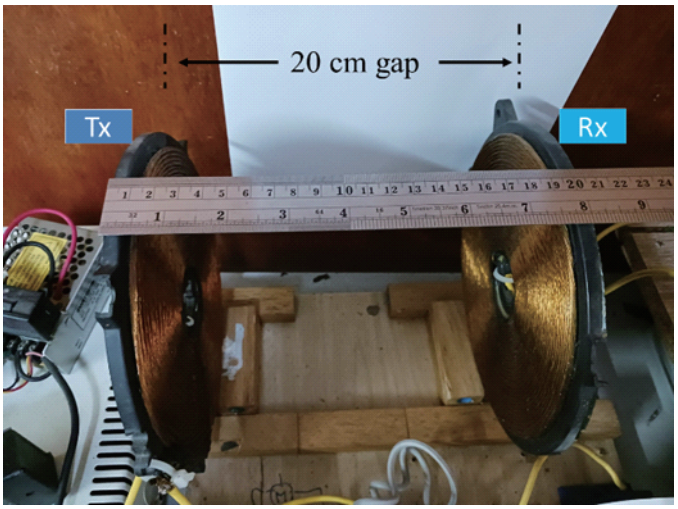

FIGURE 5. (a) Designed WPT system for analysis of temperature. (b) Air Gap between Tx and Rx.

ical requirements, cobalt is a valuable metal which is utilized in the production of materials needed for a variety of applications, including industrial catalysts, lithium-ion batteries, hard metals, magnets, and gas turbine components [59].

3. DESIGN METHODOLOGY OF CO-SI WAFER

Firstly, an aluminium sheet is utilized and designed through a laser cutting technique to deposit the cobalt film on the silicon wafer substrate.

RF magnetron sputtering technique was operated to coat Co films and connect in a zigzag manner with copper on a Si wafer substrate.

The sample surface was cleaned by applying the argon plasma ion at a flow rate of 50 cm with 25 W (DC) and 40 W (DC) for 3 minutes and 5 minutes, respectively. A 100 W (DC) power was applied to the Co target for 8 minutes ($\sim$ 10 nm) to deposit on the Silica substrate and about 3 minutes and 4 sec for the copper to deposit and connect the cobalt films in a zig-zag manner. Fig. 3 above shows the fabricated Co-Si wafer which

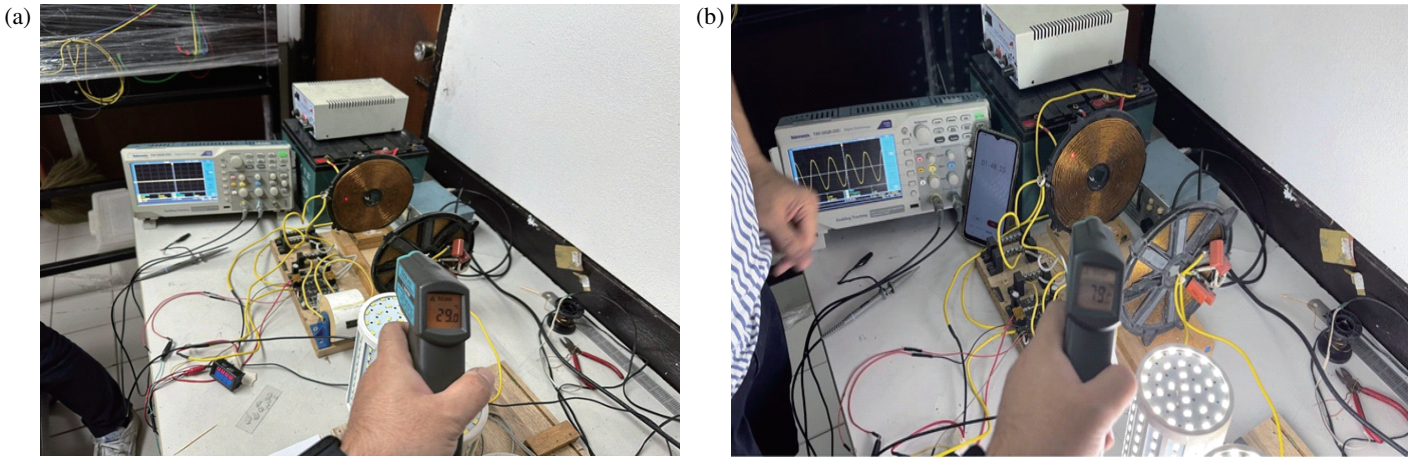

FIGURE 6. (a) Temperature analysis before the operating of WPT system. (b) Temperature analysis after operating condition at 100 seconds.

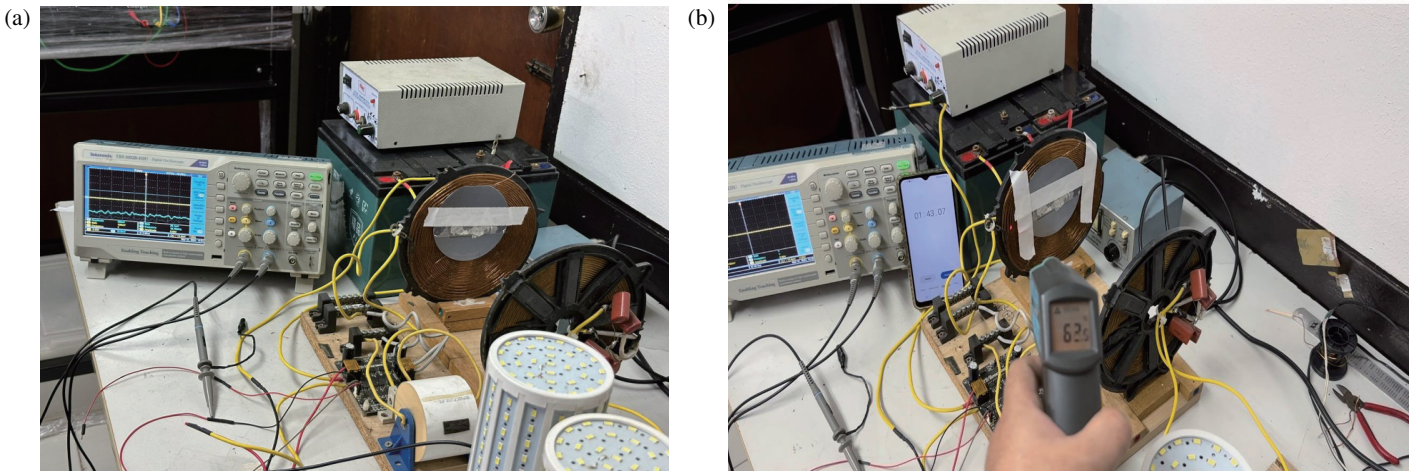

FIGURE 7. (a) WPT system with silicon cobalt wafer design. (b) Maximum temperature reach with wafer design.

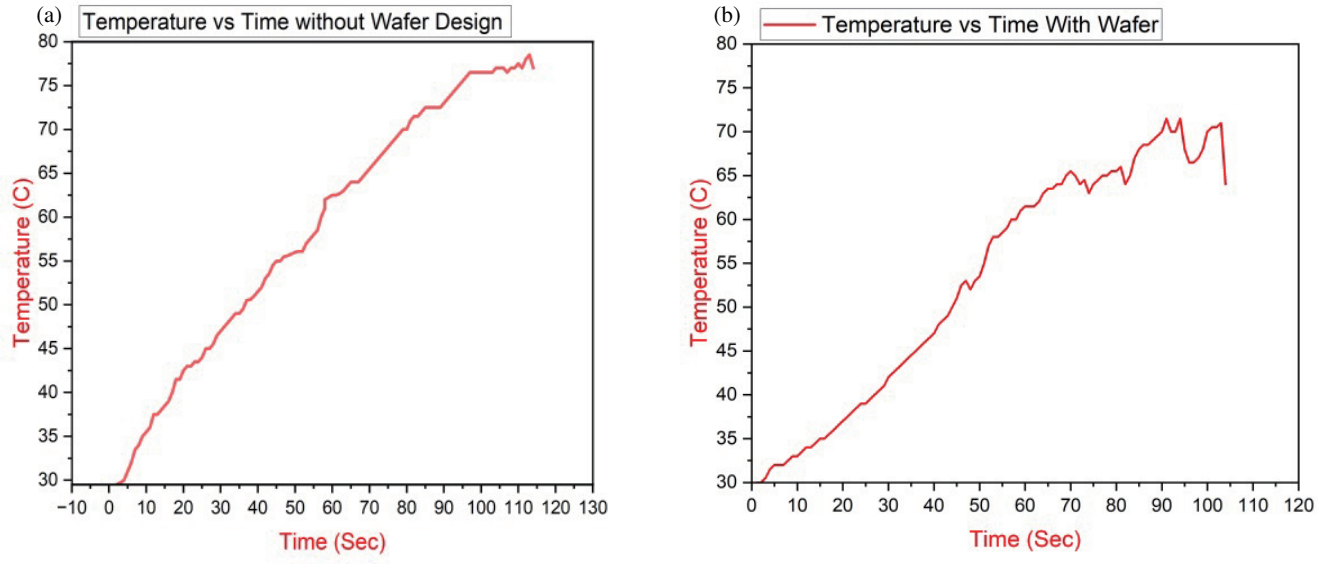

FIGURE 8. (a) Maximum temperature w.r.t time of WPT. (b) Temperature w.r.t time with of WPT setup with wafer design.

will be utilized at the TX side of the static WPT system, while measuring the SSE of the designed model is shown in Fig. 3(b).

4. EXPERIMENTAL SETUP

An experimental layout and setup of the WPT system are shown in Figs. 4 and 5(a) which consists of a high frequency (HF) H-bridge system, a power supply, and a DC to AC inverter system on the Transmitter side. In contrast, the receiver side (Rx) consists of an Rx coil AC to DC rectifier and a resonant tuning capacitor connected directly to the load while the air gap between the TX and Rx coils is shown in Fig. 5(b).

5. RESULTS AND DISCUSSIONS

The thermal performance of a wireless power transmission system shown in Figs. 6(a) and (b) is the main concern of this study. Thermal sensors monitored the magnetic coil's temperature when equipment was in operation, and it reached a maximum of 70–79°C in about 100 seconds. Temperatures above this level reduced the overall efficiency of the system by impairing the functioning of other components, even while power efficiency stayed constant. In order to minimize this effect, the magnetic coupler was coupled with a silicon wafer design shown in Figs. 7(a) and (b) which led to a significant temperature drop to 62–64°C without an apparent impact on efficiency in same time i-e 100 seconds. The results suggest that while heat rise can significantly impact system components, its effect on efficiency is limited; therefore, minimizing temperature-related component errors and achieving effective thermal control are essential. Figs. 8(a) and (b) show the accompanying graphs of temperature distribution with respect to time of the magnetic coupler in both setups i-e with and without the designed wafer model.

6. CONCLUSION

In this research, wireless power setups are arranged and analyzed to evaluate thermal performance both with and without the designed wafer. The transmission coil's temperature is compared between Si-Cobalt Wafer TX system and conventional WPT system. The working frequency was preferred to be the frequency at which it is enhanced between the transmitting and receiving coils. The Si-Cobalt wafer with the transmitter system performed better than a conventional transmission system at an air gap of 20 cm from the Rx coil. Results imply that heat rises can have significant impacts on system components, and they have a limited effect on efficiency. The graphs above illustrate the temperature distribution across various positions of the magnetic coupler. In order to minimize temperature-related component errors and accomplish efficient thermal control, it is crucial to implement effective cooling strategies and optimize the thermal management design.

ACKNOWLEDGEMENT

This Research work was supported by Thammasat University Ph.D. Scholarship as well as Thammasat University Research Unit in spin-photonic for quantum technology.

REFERENCES

[1] Mi, C. C., G. Buja, S. Y. Choi, and C. T. Rim, "Modern advances in wireless power transfer systems for roadway powered electric vehicles," *IEEE Transactions on Industrial Electronics*, Vol. 63, No. 10, 6533–6545, 2016.

[2] Ghosh, A., "Possibilities and challenges for the inclusion of the electric vehicle (EV) to reduce the carbon footprint in the transport sector: A review," *Energies*, Vol. 13, No. 10, 2602, 2020.

[3] Covic, G. A., J. T. Boys, M. L. G. Kissin, and H. G. Lu, "A three-phase inductive power transfer system for roadway-powered vehicles," *IEEE Transactions on Industrial Electronics*, Vol. 54, No. 6, 3370–3378, 2007.

[4] Keeling, N. A., J. T. Boys, and G. A. Covic, "Unity power factor inductive power transfer pick-up for high power applications," in *2008 34th Annual Conference of IEEE Industrial Electronics*, 1039–1044, Orlando, FL, USA, 2008.

[5] Budhia, M., G. Covic, and J. Boys, "A new IPT magnetic coupler for electric vehicle charging systems," in *IECON 2010-36th Annual Conference on IEEE Industrial Electronics Society*, 2487–2492, Glendale, AZ, USA, 2010.

[6] Budhia, M., G. A. Covic, and J. T. Boys, "Design and optimisation of magnetic structures for lumped inductive power transfer systems," in *2009 IEEE Energy Conversion Congress and Exposition*, 2081–2088, San Jose, CA, USA, 2009.

[7] Sun, X., Z. Li, X. Wang, and C. Li, "Technology development of electric vehicles: A review," *Energies*, Vol. 13, No. 1, 90, 2019.

[8] Miller, J. M., P. T. Jones, J.-M. Li, and O. C. Onar, "ORNL experience and challenges facing dynamic wireless power charging of EV's," *IEEE Circuits and Systems Magazine*, Vol. 15, No. 2, 40–53, 2015.

[9] Li, S., Z. Liu, H. Zhao, L. Zhu, C. Shuai, and Z. Chen, "Wireless power transfer by electric field resonance and its application in dynamic charging," *IEEE Transactions on Industrial Electronics*, Vol. 63, No. 10, 6602–6612, 2016.

[10] Kim, D., D. Jeong, J. Kim, H. Kim, J. Kim, S.-M. Park, and S. Ahn, "Design and implementation of a wireless charging-based cardiac monitoring system focused on temperature reduction and robust power transfer efficiency," *Energies*, Vol. 13, No. 4, 1008, 2020.

[11] Kim, M., K. A. Kim, J. Kim, and J.-H. Jung, "Design methodology of a 500 W wireless power transfer converter," in *2015 IEEE PELS Workshop on Emerging Technologies: Wireless Power (2015 WoW)*, 1–6, 2015.

[12] Li, W., H. Zhao, J. Deng, S. Li, and C. C. Mi, "Comparison study on SS and double-sided LCC compensation topologies for EV/PHEV wireless chargers," *IEEE Transactions on Vehicular Technology*, Vol. 65, No. 6, 4429–4439, 2015.

[13] Sohn, Y. H., B. H. Choi, E. S. Lee, G. C. Lim, G.-H. Cho, and C. T. Rim, "General unified analyses of two-capacitor inductive power transfer systems: equivalence of current-source SS and SP compensations," *IEEE Transactions on Power Electronics*, Vol. 30, No. 11, 6030–6045, 2015.

[14] Aditya, K. and S. S. Williamson, "Comparative study of series-series and series-parallel compensation topologies for electric vehicle charging," in *2014 IEEE 23rd International Symposium on Industrial Electronics (ISIE)*, 426–430, Istanbul, Turkey, 2014.

[15] Zhang, W., S.-C. Wong, K. T. Chi, and Q. Chen, "Analysis and comparison of secondary series-and parallel-compensated inductive power transfer systems operating for optimal efficiency and load-independent voltage-transfer ratio," *IEEE Transactions on Power Electronics*, Vol. 29, No. 6, 2979–2990, 2013.

[16] Stielau, O. H. and G. A. Covic, "Design of loosely coupled inductive power transfer systems," in *Powercon 2000. 2000 International Conference on Power System Technology. Proceedings (Cat. No. 00ex409)*, Vol. 1, 85–90, Perth, WA, Australia, 2000.

[17] Neath, M. J., A. K. Swain, U. K. Madawala, and D. J. Thrimawithana, "An optimal pid controller for a bidirectional inductive power transfer system using multiobjective genetic algorithm," *IEEE Transactions on Power Electronics*, Vol. 29, No. 3, 1523–1531, 2013.

[18] Wu, H. H., G. A. Covic, J. T. Boys, and D. J. Robertson, "A series-tuned inductive-power-transfer pickup with a controllable AC-voltage output," *IEEE Transactions on Power Electronics*, Vol. 26, No. 1, 98–109, 2010.

[19] Lee, S.-H., M.-Y. Kim, B.-S. Lee, and J. Lee, "Impact of rebar and concrete on power dissipation of wireless power transfer systems," *IEEE Transactions on Industrial Electronics*, Vol. 67, No. 1, 276–287, 2019.

[20] Gaona, D. E., C. Jiang, and T. Long, "Highly efficient 11.1-kW wireless power transfer utilizing nanocrystalline ribbon cores," *IEEE Transactions on Power Electronics*, Vol. 36, No. 9, 9955–9969, 2021.

[21] Budhia, M., J. T. Boys, G. A. Covic, and C.-Y. Huang, "Development of a single-sided flux magnetic coupler for electric vehicle IPT charging systems," *IEEE Transactions on Industrial Electronics*, Vol. 60, No. 1, 318–328, 2011.

[22] Xia, B., Y. Liu, R. Huang, Y. Yang, Y. Lai, W. Zheng, H. Wang, W. Wang, and M. Wang, "Thermal analysis and improvements of the power battery pack with liquid cooling for electric vehicles," *Energies*, Vol. 12, No. 16, 3045, 2019.

[23] Zhao, J., Z. Rao, Y. Huo, X. Liu, and Y. Li, "Thermal management of cylindrical power battery module for extending the life of new energy electric vehicles," *Applied Thermal Engineering*, Vol. 85, 33–43, 2015.

[24] Zhang, X., C. Liu, and Z. Rao, "Experimental investigation on thermal management performance of electric vehicle power battery using composite phase change material," *Journal of Cleaner Production*, Vol. 201, 916–924, 2018.

[25] Wang, S., M. A. D. Rooij, W. G. Odendaal, J. D. V. Wyk, and D. Boroyevich, "Reduction of high-frequency conduction losses using a planar litz structure," *IEEE Transactions on Power Electronics*, Vol. 20, No. 2, 261–267, 2005.

[26] Sallan, J., J. L. Villa, A. Llombart, and J. F. Sanz, "Optimal design of ICPT systems applied to electric vehicle battery charge," *IEEE Transactions on Industrial Electronics*, Vol. 56, No. 6, 2140–2149, 2009.

[27] Liu, J., Q. Deng, D. Czarkowski, M. K. Kazimierczuk, H. Zhou, and W. Hu, "Frequency optimization for inductive power transfer based on AC resistance evaluation in litz-wire coil," *IEEE Transactions on Power Electronics*, Vol. 34, No. 3, 2355–2363, 2018.

[28] Deng, Q., J. Liu, D. Czarkowski, M. K. Kazimierczuk, M. Bojarski, H. Zhou, and W. Hu, "Frequency-dependent resistance of litz-wire square solenoid coils and quality factor optimization for wireless power transfer," *IEEE Transactions on Industrial Electronics*, Vol. 63, No. 5, 2825–2837, 2016.

[29] Acero, J., R. Alonso, J. M. Burdio, L. A. Barragan, and D. Puyal, "Frequency-dependent resistance in litz-wire planar windings for domestic induction heating appliances," *IEEE Transactions on Power Electronics*, Vol. 21, No. 4, 856–866, 2006.

[30] Wei, G., X. Jin, C. Wang, J. Feng, C. Zhu, and M. I. Matveevich, "An automatic coil design method with modified AC resistance evaluation for achieving maximum coil-coil efficiency in WPT systems," *IEEE Transactions on Power Electronics*, Vol. 35, No. 6, 6114–6126, 2019.

[31] Petkov, R., "Optimum design of a high-power, high-frequency transformer," *IEEE Transactions on Power Electronics*, Vol. 11, No. 1, 33–42, 1996.

[32] Kral, C., A. Haumer, and T. Bauml, "Thermal model and behavior of a totally-enclosed-water-cooled squirrel-cage induction machine for traction applications," *IEEE Transactions on Industrial Electronics*, Vol. 55, No. 10, 3555–3565, 2008.

[33] Liang, C., G. Yang, F. Yuan, X. Huang, Y. Sun, J. Li, and K. Song, "Modeling and analysis of thermal characteristics of magnetic coupler for wireless electric vehicle charging system," *IEEE Access*, Vol. 8, 173 177–173 185, 2020.

[34] Niu, S., H. Yu, S. Niu, and L. Jian, "Power loss analysis and thermal assessment on wireless electric vehicle charging technology: The over-temperature risk of ground assembly needs attention," *Applied Energy*, Vol. 275, 115344, 2020.

[35] Mohammad, M., O. C. Onar, J. L. Pries, V. P. Galigekere, G.-J. Su, and J. Wilkins, "Thermal analysis of a 50 kW three-phase wireless charging system," in *2021 IEEE Transportation Electrification Conference & Expo (ITEC)*, 1–6, Chicago, IL, USA, 2021.

[36] Moghaddami, M. and A. Sarwat, "Time-dependent multiphysics analysis of inductive power transfer systems," in *2018 IEEE Transportation Electrification Conference and Expo (ITEC)*, 130–134, Long Beach, CA, USA, 2018.

[37] Campi, T., S. Cruciani, V. D. Santis, and M. Feliziani, "Emf safety and thermal aspects in a pacemaker equipped with a wireless power transfer system working at low frequency," *IEEE Transactions on Microwave Theory and Techniques*, Vol. 64, No. 2, 375–382, 2016.

[38] Xiao, C., S. Hao, D. Cheng, and C. Liao, "Safety enhancement by optimizing frequency of implantable cardiac pacemaker wireless charging system," *IEEE Transactions on Biomedical Circuits and Systems*, Vol. 16, No. 3, 372–383, 2022.

[39] Kim, H., C. Song, D.-H. Kim, D. H. Jung, I.-M. Kim, Y.-I. Kim, J. Kim, S. Ahn, and J. Kim, "Coil design and measurements of automotive magnetic resonant wireless charging system for high-efficiency and low magnetic field leakage," *IEEE Transactions on Microwave Theory and Techniques*, Vol. 64, No. 2, 383–400, 2016.

[40] Ibrahim, A. and M. Kiani, "A figure-of-merit for design and optimization of inductive power transmission links for millimeter-sized biomedical implants," *IEEE Transactions on Biomedical Circuits and Systems*, Vol. 10, No. 6, 1100–1111, 2016.

[41] Bosshard, R., J. W. Kolar, J. Muhlethaler, I. Stevanovic, B. Wunsch, and F. Canales, "Modeling and η-α-pareto optimization of inductive power transfer coils for electric vehicles," *IEEE Journal of Emerging and Selected Topics in Power Electronics*, Vol. 3, No. 1, 50–64, 2014.

[42] Bosshard, R. and J. W. Kolar, "Multi-objective optimization of 50 kW/85 kHz IPT system for public transport," *IEEE Journal of Emerging and Selected Topics in Power Electronics*, Vol. 4, No. 4, 1370–1382, 2016.

[43] DiSalvo, F. J., "Thermoelectric cooling and power generation," *Science*, Vol. 285, No. 5428, 703–706, 1999.

[44] Bell, L. E., "Cooling, heating, generating power, and recovering waste heat with thermoelectric systems," *Science*, Vol. 321, No. 5895, 1457–1461, 2008.

[45] Sundarraj, P., D. Maity, S. S. Roy, and R. A. Taylor, "Recent advances in thermoelectric materials and solar thermoelectric generators – A critical review," *RSC Advances*, Vol. 4, No. 87, 46 860–46 874, 2014.

[46] Rowe, D. M., *CRC Handbook of Thermoelectrics*, CRC Press, 2018.

[47] Goldsmid, H. J., *Introduction to Thermoelectricity*, Springer, 2010.

[48] Cadeville, M. C. and J. Roussel, "Thermoelectric power and electronic structure of dilute alloys of nickel and cobalt with D transition elements," *Journal of Physics F: Metal Physics*, Vol. 1, No. 5, 686, 1971.

[49] Gravier, L., S. Serrano-Guisan, F. Reuse, and J.-P. Ansermet, "Thermodynamic description of heat and spin transport in magnetic nanostructures," *Physical Review B — Condensed Matter and Materials Physics*, Vol. 73, No. 2, 024419, 2006.

[50] Tsyplyatyev, O., O. Kashuba, and V. I. Fal'ko, "Thermally excited spin current and giant magnetothermopower in metals with embedded ferromagnetic nanoclusters," *Physical Review B — Condensed Matter and Materials Physics*, Vol. 74, No. 13, 132403, 2006.

[51] Hatami, M., G. E. W. Bauer, Q. Zhang, and P. J. Kelly, "Thermal spin-transfer torque in magnetoelectronic devices," *Physical Review Letters*, Vol. 99, No. 6, 066603, 2007.

[52] Xiao, J., G. E. W. Bauer, K.-C. Uchida, E. Saitoh, and S. Maekawa, "Theory of magnon-driven spin seebeck effect," *Physical Review B — Condensed Matter and Materials Physics*, Vol. 81, No. 21, 214418, 2010.

[53] Adachi, H., K.-I. Uchida, E. Saitoh, and S. Maekawa, "Theory of the spin seebeck effect," *Reports on Progress in Physics*, Vol. 76, No. 3, 036501, 2013.

[54] Rezende, S. M., R. L. Rodriguez-Suarez, R. O. Cunha, A. R. Rodrigues, F. L. A. Machado, G. A. F. Guerra, J. C. L. Ortiz, and A. Azevedo, "Magnon spin-current theory for the longitudinal spin-seebeck effect," *Physical Review B*, Vol. 89, No. 1, 014416, 2014.

[55] Valenzuela, S. O. and M. Tinkham, "Direct electronic measurement of the spin hall effect," *Nature*, Vol. 442, No. 7099, 176–179, 2006.

[56] Kimura, T., Y. Otani, T. Sato, S. Takahashi, and S. Maekawa, "Room-temperature reversible spin hall effect," *Physical Review Letters*, Vol. 98, No. 15, 156601, 2007.

[57] Hoffmann, A., "Spin hall effects in metals," *IEEE Transactions on Magnetics*, Vol. 49, No. 10, 5172–5193, 2013.

[58] Sinova, J., S. O. Valenzuela, J. Wunderlich, C. H. Back, and T. Jungwirth, "Spin hall effects," *Reviews of Modern Physics*, Vol. 87, No. 4, 1213–1260, 2015.

[59] Rominiyi, A. L., M. B. Shongwe, and B. J. Babalola, "Development and characterization of nanocrystalline cobalt powder prepared via high energy ball milling process," in *IOP Conference Series: Materials Science and Engineering*, Vol. 430, No. 1, 012029, 2018.